Effects of Rotor Air-gap Eccentricity on the Power Factor of Squirrel Cage Induction Machines

H. Meshgin-Kelk , J. Milimonfared

Electric Machines and Drive Laboratory
Department of Electrical Engineering
Amirkabir University of Technology
Tehran 15914, Iran
Phone: +98 (21) 646-6009
Fax: +98 (21) 640-6469
E-mail: meshgin@cic.aku.ac.ir

***Abstract*- A substantial portion of induction machine faults is eccentricity related. In this paper, we have studied the power factor variation of induction machines due to the static and dynamic eccentricities. According to this study, air-gap asymmetry leads to inductance coefficient variations and, consequently, induction machine power factor variation. Experimental results are also provided to verify the simulations.**

Keywords: induction motor, power factor, air gap eccentricity, and magnetic equivalent circuit

1. Introduction

Eccentricity is a common problem in induction machines. It is well known that an inherent level of static eccentricity exists in induction machines due to the manufacturing and assembly methods [1]. In general, there are two types of air-gap eccentricity, i.e., static and dynamic. In both, the axis of rotor is not on the axis of stator. In fact, axis of rotation is the axis of rotor, in static air-gap eccentricity; yet, it is not in dynamic air-gap eccentricity. These air-gap asymmetries produce unique signature patterns in the stator current. Furthermore, they create Unbalanced Magnetic Pulls (UMP) that cause mechanical vibration of the motor frame. Previous works done by many researchers have mostly focused on the detection of these types of asymmetries [1-6]. In deed, less attention has been paid to the performance of motor and power factor degradation due to these asymmetries. In this paper, we study the variations of inductance coefficients and power factor of induction motor due to the air-gap eccentricities. Analysis is based on our simplified magnetic equivalent circuit approach. Experimental results are also provided.

2. Derivation of Inductance Equations

The well-known relation between currents and flux linkages in an induction machine are written as the following equations:

$$L_{ss} i_s + L_{sr} i_r = \lambda_s \quad (1)$$

$$L_{rs} i_s + L_{rr} i_r = \lambda_r \quad (2)$$

where i is the current vector, λ is the flux linkage vector, L is the matrix of inductance, and subscripts s and r are assigned to stator and rotor, respectively. To study the subject of this paper first we need to derive appropriate equations for machine inductances.

In Fig.1, a part of Magnetic Equivalent Circuit (MEC) model of an induction machine is shown. To formulate the system of algebraic machine equations, nodal analysis technique that satisfies magnetic flux continuity is applied. The node potential equations for the network of Fig. 1 are given as

$$A_{11} u_1 = -\Phi_{st} \quad (3)$$

$$A_{22} u_2 + A_{23} u_3 = \Phi_{st} \quad (4)$$

$$A_{32} u_2 + A_{33} u_3 = \Phi_{rt} \quad (5)$$

$$A_{44} u_4 = -\Phi_{rt} \quad (6)$$

$$u_2 = u_1 - R_{st} \Phi_{st} + F_{st} \quad (7)$$

$$u_3 = u_4 - R_{rt} \Phi_{rt} + F_{rt} \quad (8)$$

where u_1, u_2 ,u_3, and u_4 are the vectors of magnetic node potential in stator back iron, stator teeth, rotor teeth, and rotor back iron, respectively. Also Φ_{st} and Φ_{rt} are the vectors of stator and rotor tooth fluxes, R_{st} and R_{rt} are the stator and rotor tooth reluctance matrices, F_{st} and F_{rt} are the vectors of mmf sources in stator side and rotor side, respectively. A_{11}, A_{22}, A_{23}, A_{32}, A_{33}, and A_{44} are node permeance matrices. The elements of A_{11} and A_{44} matrices depend only on stator and rotor back iron segment permeances of Fig. 1, respectively. In Fig. 1, these permeances are shown by $G_{sy,i}$ and $G_{ry,j}$. The elements of A_{22}, A_{23}, A_{32}, and A_{33} depend on stator slot, rotor slot and air-gap permeances. G_{ss} is stator slot opening leakage permeance and is a constant. $G_{rs,j}$ is rotor slot leakage permeance of slot j, and for closed slot, due to saturation effect, it is a nonlinear permeance. G_{ij} is the air-gap permeance between stator tooth i and rotor tooth j. G_{ij} is the most important parameter in magnetic equivalent circuit modeling. Derivative of air-gap permeance between stator tooth i and rotor tooth j with respect to rotor angle when multiplied by the square of mmf drop over the same permeance gives the value of electromagnetic force between them. If there are n_s stator teeth and n_r rotor teeth the number of air-gap permeances are ($n_s n_r$). But most of these permeances will be zero since in any instant of time each rotor tooth can face only a few stator teeth and vice versa.

The magnitude of G_{ij} between stator tooth *i* and rotor tooth *j* is directly proportional to the common area and is inversely proportional to the air-gap length of stator tooth *i* and rotor tooth *j* when these two face each other.

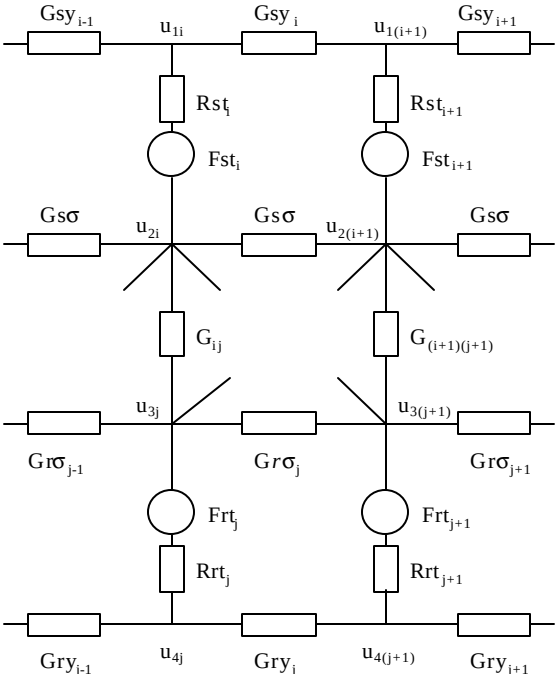

Fig1. A part of MEC model of an induction machine.

F_{st} and F_{rt} vectors in equations (7) and (8) are related to stator phase currents and rotor mesh currents through the following equations,

$$F_{st} = W_s i_s \quad (9)$$

$$F_{rt} = W_r i_r \quad (10)$$

where W_s is generated using the same approaches presented in [2] or [7]. W_s is called magneto-motive force transform matrix and depends on stator winding configuration and number of turns per coil of stator windings. W_r is an identity matrix and its size depends on the number of independent rotor mesh currents i_r.

In an induction machine the geometric shapes of yoke parts are such that they have large cross section area and nearly short length with respect to tooth parts of stator and rotor. Fig. 2 shows a typical rotor lamination of an induction machine. Therefore, mmf drops on these yoke parts are generally several times smaller than mmf drops on tooth parts. It should be noted that in Magnetic Equivalent Circuit model, direction of fluxes in a tooth and in a yoke segment are perpendicular to each other. Although yoke parts reluctances have some effects on machine inductances, simulation results show that neglecting mmf drops on yoke parts has small effects on motor inductance coefficients. Also it is possible to change the values of tooth reluctances by some percent to compensate the removal of yoke reluctances.

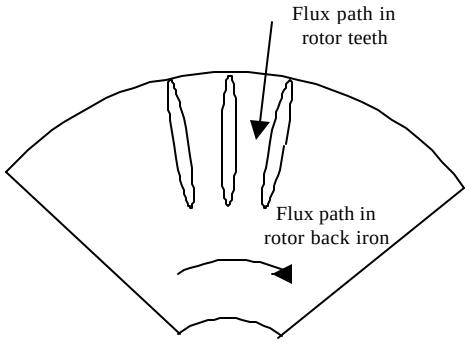

Fig. 2 A typical rotor lamination.

Neglecting back iron reluctances in the stator leads to equality of u_1 elements and neglecting back iron reluctances in the rotor leads to equality of u_4 elements. On the other hand, due to the fact that:

$$\sum_{i=1}^{n_s} \Phi_{st_i} = 0 \quad \text{and} \quad \sum_{j=1}^{n_r} \Phi_{rt_j} = 0 \quad (11)$$

Therefore, u_1 and u_4 are zero vectors and equations (7) and (8) reduce to:

$$u_2 = -R_{st}\Phi_{st} + W_s i_s \quad (12)$$

$$u_3 = -R_{rt}\Phi_{rt} + i_r \quad (13)$$

The result of such assumptions lead to removal of equations (3) and (6) from the system of algebraic equation of magnetic equivalent circuit model of induction machine (equations (3) through (10)).

By substituting (9), (10), (12), and (13) in (4) and (5), and then rearranging of parameters, we have:

$$A_{22}W_s i_s + A_{23} i_r = (\mathrm{I}_{ns\times ns} + A_{22}R_{st})\Phi_{st} + A_{23}R_{rt}\Phi_{rt} \quad (14)$$

$$A_{32}W_s i_s + A_{33} i_r = (\mathrm{I}_{nr\times nr} + A_{33}R_{rt})\Phi_{rt} + A_{32}R_{st}\Phi_{st} \quad (15)$$

By introducing matrices C and D as follows:

$$C = (\mathrm{I}_{ns\times ns} + A_{22}R_{st})^{-1}$$

$$D = (\mathrm{I}_{nr\times nr} + A_{33}R_{rt})^{-1}$$

and by further simplification the following equations will be obtained,

$$C \cdot A_{22}W_s i_s + C \cdot A_{23} i_r = \Phi_{st} + C \cdot A_{23}R_{rt}\Phi_{rt} \quad (16)$$

$$D \cdot A_{32}W_s i_s + D \cdot A_{33} i_r = \Phi_{rt} + D \cdot A_{32}R_{st}\Phi_{st} \quad (17)$$

Multiplying the two sides of (16) by ${W_s}^T$ and defining the right hand side of the result as the entire stator flux linkage and also defining the right hand side of (17) as $\boldsymbol{l}_r$, the following will be obtained:

$${W_s}^T CA_{22}W_s i_s + {W_s}^T CA_{23} i_r = \boldsymbol{l}_s \quad (18)$$

$$D \cdot A_{32}W_s i_s + D \cdot A_{33} i_r = \boldsymbol{l}_r \quad (19)$$

Comparing these equations with (1) and (2) results in

$$L_{ss} = W_s{}^T C A_{22} W_s \quad (20)$$

$$L_{sr} = W_s{}^T C A_{23} \quad (21)$$

$$L_{rs} = D A_{32} W_s \quad (22)$$

$$L_{rr} = D A_{33} \quad (23)$$

Most of elements in Matrices A_{22}, A_{23}, A_{32} and A_{33} are dependent to air-gap permeances between each stator tooth and each rotor tooth. For an eccentric rotor, air gap permeances depend on relative position of these teeth and type of eccentricity. Using equations (20-23), one can calculate various inductance coefficients with respect to the variation of air-gap length.

3. Calculation of Inductance Coefficients (Linear Magnetic Characteristic)

According to derived equations, inductance coefficients of a 3-hp three-phase induction motor with the parameters given in Appendix I have been calculated with respect to the variation of air-gap length. Table 1 and Fig. 3 show the variation of average of L_{aa} (self-inductance of phase a) with respect to the level of static and dynamic eccentricity. A linear magnetic curve has been considered. These results show that as the level of both types of eccentricity increase, average values of these inductances increase that lead to power factor improvement of motor.

Table 1 Average values of stator self and mutual inductance extracted from derived equations

	STATIC ECCENTRICITY		DYNAMIC ECCENTIRICITY	
Level of eccentricity(%)	L_{aa} (inH)	L_{ab} (inH)	L_{aa} (in H)	L_{ab} (in H)
0	.3572	-.1480	.3572	-.1480
20	.3645	-.1511	.3645	-.1511
40	.3895	-.1620	.3896	-.1615
60	.4450	-.1883	.4463	-.1851
80	.5867	-.2691	.5948	-.2469

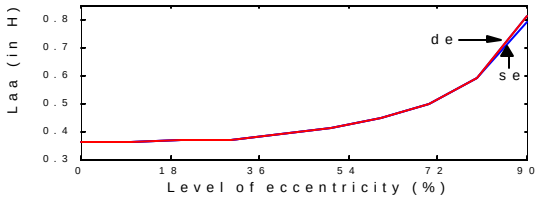

Fig.3 Variation of (Laa) vs level of air gap eccentricity (de: dynamic eccentricity, se : static eccentricity)

4. Power Factor Consideration

The IEEE Standard 112 steady state model of an induction machine is appropriate for power factor consideration. Fig 4 shows this model.

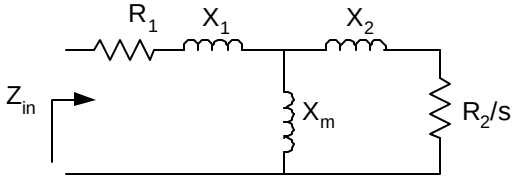

Fig 4 Steady state model of an induction machine

For our purpose, approximate model of induction machine model is sufficient. By neglecting the stator impedance and the rotor leakage reactance (that is more valid especially in no-load condition), i.e.

$$R_1 + jX_1 \approx 0 \quad (24)$$

$$X_2 << (R_2 / s) \quad (25)$$

input impedance of induction motor is obtained as follows:

$$Z_{in} = \frac{j\frac{R_2}{s} X_m}{\frac{R_2}{s} + jX_m} \quad (26)$$

where the angle of input impedance is

$$f = \angle Z_{in} = 90 - \tan^{-1}\left(\frac{X_m}{R_2/s}\right) \quad (27)$$

In steady state condition, power factor of induction machine is the cosine of f,

$$pf = \cos f \quad (28)$$

It is clearly seen that by increasing the value of X_m, the angle of Z_{in} decreases and this in turn leads to higher power factor. As shown before, air-gap eccentricity increases the stator self-inductances and therefore increases the magnitude of magnetizing inductance. Therefore higher air-gap eccentricity leads to higher power factor.

5. Complete system of differential and algebraic equations of an induction machine

Part 1. Differential Equations

The well-known differential system of equations of an induction machine is

$$v_s = R_s i_s + \frac{d\boldsymbol{l}_s}{dt} \quad (29)$$

$$v_r = R_r i_r + \frac{d\boldsymbol{l}_r}{dt} \quad (30)$$

where v *is* the voltage vector, i is the current vector, $\boldsymbol{l}$ is the flux linkage vector, R is the matrix of resistance and subscripts s and r are assigned to stator and rotor, respectively. For stator, v_s and i_s are as the following:

$$v_s = [v_a \quad v_b \quad v_c]^T$$

$$i_s = [i_a \quad i_b \quad i_c]^T$$

where *a, b,* and *c* denote for phase quantities.

Stator differential equation can be converted from phase quantities into line-line quantities. This can be done by subtraction of row 2 from row 1 and row 3 from row 2 in equation (29). These subtractions correspond to multiplying both sides of equation (29) by a transform matrix M_{yn} that has the following form:

$$M_{yn} = \begin{bmatrix} 1 & -1 & 0 \\ 0 & 1 & -1 \end{bmatrix}$$

For rotor, v_r and i_r are as the following:

$$v_r = [v_{r1} \quad \ldots \quad v_{rj} \quad \ldots \quad v_{rn_r}]^T$$

$$i_r = [i_{r1} \quad \ldots \quad i_{rj} \quad \ldots \quad i_{rn_r}]^T$$

where for a cage induction motor v_r is a zero voltage vector, and i_r is the vector of rotor mesh currents. n_r is the number of independent rotor mesh currents.

The mechanical differential equations of an induction machine are

$$T_e - T_m = J\frac{d\boldsymbol{w}}{dt} \quad (31)$$

$$\boldsymbol{w} = \frac{d\boldsymbol{q}}{dt} \quad (32)$$

$$T_e = \sum_{i=1}^{n_s}\sum_{j=1}^{n_r}(u_{2_i} - u_{3_j})^2 . \frac{dg_{ij}}{d\boldsymbol{q}} \quad (33)$$

where T_e is electromechanical torque of machine, T_m is load torque, $\boldsymbol{q}$ is the mechanical angle, J is the inertia, $\boldsymbol{w}$ is mechanical speed, and $(dg_{ij}/d\boldsymbol{q})$ is the derivative of air gap permeances with respect to mechanical angle.

Part 2. Complete System of Algebraic Equations

Algebraic equations of an induction machine in matrix notation are as the following

$$\begin{bmatrix} M_0 & 0 & 0 \\ M_{yn}W_s^T A_{22}W_s & M_{yn}W_s^T A_{23} & -M_{yn}W_s^T A_{22}R_{st} \\ A_{22}W_s & A_{23} & -(I_{n_s} + A_{22}R_{st}) \\ A_{32}W_s & A_{33} & -A_{32}R_{st} \end{bmatrix} \begin{bmatrix} i_s \\ i_r \\ \Phi_{st} \end{bmatrix} = \begin{bmatrix} 0 \\ M_{yn}l_s + M_{yn}W_s^T A_{23}R_{rt}\Phi_{rt} \\ R_{rt}\Phi_{rt} \\ (I_{n_r} + A_{33}R_{rt})\Phi_{rt} \end{bmatrix} \quad (34)$$

$$u_2 = -R_{st}\Phi_{st} + W_s i_s \quad (35)$$

$$u_3 = -R_{rt}\Phi_{rt} + i_r \quad (36)$$

M_0 is a matrix that reflects the type of winding connection (delta, star, with or without a neutral connection). For example, for a three-phase star connected without neutral, M_0 is as the following:

$$M_0 = [1 \quad 1 \quad 1]$$

6. Simulation (Nonlinear BH Curve) and Power Factor Measurement

Using the proposed method , a 3-hp motor has been modeled and simulated. To obtain more accurate results, a nonlinear BH curve has been considered. A healthy operation as well as an static eccentric operation has been studied. Zero crossings of the phase voltages and currents have been used for the power factor calculation, in simulations and experiments.

Average values of power factor from simulation as well as experimental results for a healthy and a static eccentric operation (nearly 70%) under no-load and full load operations are shown in table 2. In spite of some difference between simulation and measured results, they confirmed each other. It can be seen that average of power factor in healthy motor in no load operation is lower with respect to eccentric rotor.

Table 2 calculated and measured power factor

	Simulation		Experiment	
	No-load	Full-load	No-load	Full-load
Healthy motor	0.32	0.836	0.263	0.85
70% SEC	0.483	0.864	0.493	0.845

Inductance coefficients depend on the stator and rotor fluxes especially when there is deep saturation (refer to equations (20)-(23), since they depend to stator and rotor reluctances through matrices *C* and *D*). Fig. 5 depicts this variation obtained from an on-line starting of motor in a complete simulation. This figure shows the variation of L_{aa} with respect to the rotor position in one rotor revolution that has been calculated in each step of simulation. As is shown, average of L_{aa} in steady state condition (0.3810 H for 40% static eccentricity) is very close to the similar case (0.3895 H)

calculated with a linear magnetic curve (Table 1). Of course for deep saturation in steady state, reduction of the average value of L_{aa} is higher with respect to our simulation conditions.

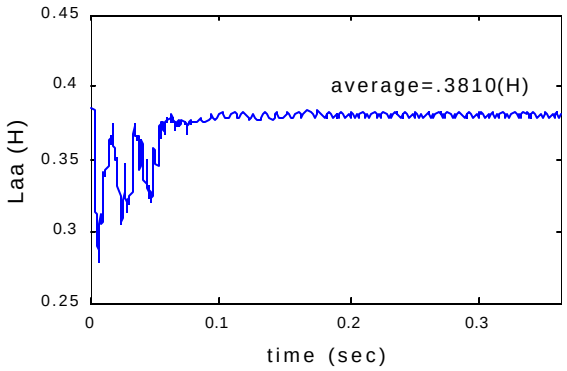

Fig. 5 Variation of (Laa) for 40% static eccentricity after on-line starting

7. Conclusion

In this paper the equations describing motor inductance coefficients including most important features of induction motor have been derived. According to these equations, variation of motor inductances and therefore motor power factor with respect to the level air-gap eccentricity has been studied. Using the proposed method an induction motor has been simulated. Variation of stator self-inductance in an on-line start up operation including saturation effect has been represented. To verify the theoretical aspects experimental results have been provided.

Appendix I

Machine Parameters
Three hp, 460/230V, 4 pole
Rotor length = 2 in
Stator slot opening: 0.12 in
Inner stator diameter = 4.875 in; Air-gap length = 0.013 in
Number of stator slots, n_s = 36; Number of rotor slots, n_r = 44
Stator winding configuration: single layer concentrated winding and number of coil per slot N=54
Stator resistance: Rs = 3.7 Ω/phase
Rotor bar resistance: Rb =50.06 μΩ
Rotor end ring resistance: Re = 2.6748 μΩ
Inertia: 0.0113 for no-load condition

References

[1] D. G. Dorrell, W. T. Thomson, and S. Roach, "Analysis of air-gap flux, current, and vibration signals as a function of combination of static and dynamic air-gap eccentricity in 3-phase induction motors" IEEE Trans. on Industry Applications, vol. 33, no. 1, Jan./Feb. 1997.
[2] H. A. Toliyat, M. S. Arefeen, and A. G. Parlos, "A method for dynamic simulation of air-gap eccentricity in induction machines" IEEE Trans. on Industry Applications, vol. 32, no. 4, pp. 910-918, July/Aug. 1996.
[3] J. R. Cameron, W. T. Thomson, and A. B. Dow, "Vibration and current monitoring for detecting air-gap eccentricity in large induction motors", IEE Proceedings, vol. 133, pt. B, no. 3, pp. 155-163, May 1986.
[4] S. Nandi, R. Bharadwaj, H. A. Toliyat, and A. G. Parlos, "Performance analysis of a three induction motor under mixed eccentricity condition", IEEE 1998, Pages 123-128.
[5] J. M. Cardoso and E. S. Saraiva, "Predicting the level of air-gap eccentricity in operating three phase induction motor, by Park's vector approach", Proc. of the Industry Applications Society Annual Meeting, 1992, pp. 132 –135.
[6] J. M. Cardoso, E. S. Saraiva, M. L. S. Mateus, and A. L. Ramalho, "On-line detection of air-gap eccentricity in 3-phase induction motor, by Park's vector approach", Proc. of the 5th International Conference on Electrical Machines and Drives, 1991, pp. 61-66.
[7] V. Ostovic, Dynamics of saturated electric machines, Springer Verlag, New York, 1989.